



AIAA 96-3392

High Angle of Attack Missile Aerodynamics
Including Rotational Rates - Program M3HAX

D. Lesieutre, J. Love, and M. Dillenius
Nielsen Engineering & Research, Inc.
Mountain View, CA

Atmospheric Flight Mechanics Conference
July 29 - 31, 1996 / San Diego, CA

For permission to copy or republish, contact the copyright owner named on the first page.

For AIAA-held copyright, write to AIAA Permissions Department,
1801 Alexander Bell Drive, Suite 500, Reston, VA, 20191-4344.

High Angle of Attack Missile Aerodynamics Including Rotational Rates - Program *M3HAX*

Daniel J. Lesieutre^{*}, John F. Love[†], Marnix F. E. Dillenius[‡]
Nielsen Engineering and Research, Inc.
Mountain View, CA 94043

ABSTRACT

The engineering-level missile aerodynamic prediction code *M3F3CA* has been extended from a maximum angle of attack limit of 45° up to 90°. In addition, the equivalent angle of attack methodology employed has been extended to include the effects of rotational rates and nonuniform flow effects. The new prediction code is designated *M3HAX*. The program is based on the equivalent angle of attack methodology and various experimental data bases to predict the longitudinal and lateral-directional aerodynamic characteristics of missiles at angles of attack up to 90°. The new methodology used to extend the prediction program to 90° angle of attack and to include rotational rate and nonuniform effects is described. Comparisons to independent experimental data are presented to demonstrate the unique qualities of the code. In general, good agreement with experimental data is obtained for a variety of configurations (body alone, single fin set, 2 fin set, and 3 fin set configurations) and flow conditions (symmetric and asymmetric).

LIST OF SYMBOLS

AR	aspect ratio (two fins joined at root)
C_{BM}	fin bending moment/ $q_{\infty} S_R l_R$
C_{dc}	body crossflow drag coefficient
C_{HM}	fin hinge moment/ $q_{\infty} S_R l_R$
C_l	rolling moment/ $q_{\infty} S_R l_R$
C_{lp}	roll-damping coefficient; $\partial C_l / \partial (pb/2V_{\infty})$
C_m	pitching-moment/ $q_{\infty} S_R l_R$; positive nose up
C_{mq}	pitch-damping derivative; $\partial C_m / \partial (ql_R/2V_{\infty})$
$C_{m\alpha}$	plunge-damping derivative; $\partial C_m / \partial (\alpha l_R/2V_{\infty})$
C_N	normal force/ $q_{\infty} S_R$
C_{NF}	fin normal force/ $q_{\infty} S_R$
$C_{N\alpha}$	body $dC_N/d\alpha$ at $\alpha=0$
l_R	reference length
s	exposed fin span
s_m	fin semispan measured from body centerline

S_R	reference area
x_{mc}, x_{cg}	moment center
α_c	included angle of attack
λ	fin taper ratio
ϕ	roll angle

INTRODUCTION

An engineering-level prediction method has been developed for aerodynamic performance prediction and for preliminary design of conventional missiles with cruciform fin sections.¹⁻⁴ The method uses the Triservice systematic fin-on-body force and moment data base^{2,5} which covers a Mach number range from 0.6 to 4.5, fin aspect ratios from 0.25 to 4.0, angles of attack up to $\pm 45^\circ$, arbitrary roll angles, and deflection angles from -40° to 40° . The method uses the equivalent angle of attack concept which includes the effects of vorticity and geometric scaling. The latest program described here is designated *M3HAX*.¹ Program *M3HAX* has been developed by extending the *M3F3CA* code² to angles of attack up to 90° and by including rotational rate effects and nonuniform flow field effects. The *M3F3CA* program extended the previous MISL3 code³ to include an axial force prediction, to allow three fin sets, up to four fins in a set, and high aspect ratio fins. The range of parameters allowed by program *M3HAX* is summarized in Table 1 below.

Flow Conditions:	
$0.5 \leq M_{\infty} \leq 5.0$	$-90^\circ \leq \alpha_c \leq 90^\circ$
arbitrary roll angle	$-40^\circ \leq \delta \leq 40^\circ$
arbitrary rotational rates (p,q,r)	
user specified nonuniform flow field	
Geometries:	
$0.25 \leq AR \leq 10.0$	$0.0 \leq \lambda \leq 1.0$
up to three finned sections	1 to 4 fins per finned section
identical fins within a section	symmetrical airfoil sections
no fins with forward sweep	no fin trailing edge sweep

Table 1. Range of Parameters

^{*}Senior Research Engineer, Snior Member AIAA

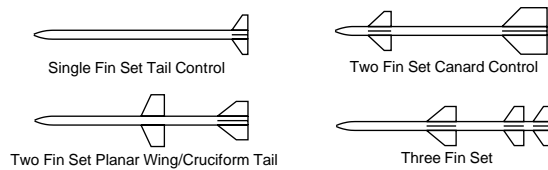
[†]Research Engineer

[‡]President, Associate Fellow AIAA

Copyright ©2002 by Nielsen Engineering & Research, Inc.

Published by the American Institute of Aeronautics and Astronautics, Inc. with permission.

Some examples of configurations addressable by *M3HAX* are shown in the next sketch.



The technical approach section of this paper summarizes the experimental and analytical data bases included in the *M3HAX* program and describes the equivalent angle of attack methodology including the inclusion of rotational rate and nonuniform flow effects. Extensive comparisons to independent experimental data for a variety of configurations and flow conditions are presented, and conclusions and recommendations are given.

TECHNICAL APPROACH

This section summarizes the experimental and analytical data bases used within the *M3HAX* program and describes the body and fin force and moment calculations.

Overview of Data Bases Within *M3HAX*

The Triservice experimental data bases cover the M_∞ range from 0.6 to 4.5, α_c up to 45° , and arbitrary roll angles. Table 2 below depicts the AR and λ domain of the fin-on-body and wing-alone data bases included in *M3HAX*. The numbers in Table 2 are the fin designation numbers. Figure 1 depicts these fins. The body radius to fin semispan ratio, a/s_m , is 0.5 for the triservice experimental data. The equivalent angle of attack methodology described later is used to scale results to other a/s_m .

AR	Taper Ratio, λ			
	0	1/2	1	
1/4		12		Triservice Experimental Data Base
1/2	31	32	33	
1		42		
2	51	52	53	Control Data
4		62		
6	71	72	73	Analytic Extension
10		82		

Table 2. AR and λ Range of *M3HAX* Data Bases

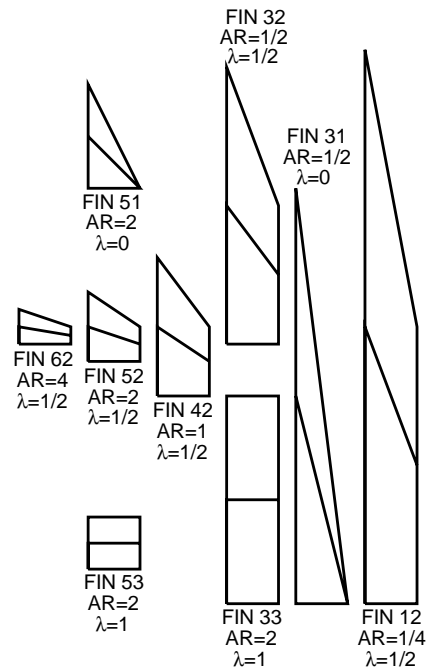


Figure 1.- Triservice data base fins

Fin Stability Data Base. The stability data base consists of fin normal force, $C_{NF}(AR, \lambda, M_\infty, \alpha_c, \phi_f)$ and centers of pressure, $x_{CP}(AR, \lambda, M_\infty, C_{NF})/c_R$ and $y_{CP}(AR, \lambda, M_\infty, C_{NF})/s$.

Fin Control Data Base. Fins with AR from 1 to 4 are deflectable control fins. For transonic Mach numbers ($M_\infty \leq 1.2$), the Triservice data base is employed; that is, $C_{NF}(AR, \lambda, M_\infty, \alpha_c, \phi_f, \delta)$, $x_{cp}(AR, \lambda, M_\infty, C_{NFD})/c_R$, and $y_{CP}(AR, \lambda, M_\infty, C_{NFD})/s$ for $a/s_m = 0.5$. For supersonic Mach numbers interference effects and control effectiveness are handled by slender body theory.

Wing-Along Data Base. A wing-alone data base, required by the equivalent angle of attack method, is composed of normal-force coefficient data for $0^\circ \leq \alpha_c \leq 90^\circ$ and $0.6 \leq M_\infty \leq 4.5$. The AR and λ range for this data base are the same as those for the fin stability data base described above. The wing-alone curves were generated from various sources.^{6,7} Recently obtained wing-alone data⁸ is currently being investigated for inclusion in the *M3HAX* prediction code.

High Aspect Ratio Fins in *M3HAX*. The AR range of the fins in the Triservice experimental data base incorporated in *M3HAX* is from 0.25 to 4. For AR in excess of 4, systematic data for fin-on-body aerodynamic forces and moments and wing-alone C_{NW} are not readily available for direct use in *M3HAX*.

Therefore, methods based on elements of subsonic and supersonic linear theory with nonlinear additions were used in conjunction with available experimental data to extend the data bases up to an AR of 10.²

Fin and Body Data Used at 90° Angle of Attack.

Program *M3HAX* uses a component buildup approach to determine the aerodynamic characteristics of a missile. The methods used in *M3F3CA*² for determining the loads on the individual components were extended or modified to include angles of attack up to 90°, angular rates, and nonuniform flow fields. In *M3HAX* a sectional body load calculation is used to capture the variation in local conditions along the body length due to angular rates and a nonuniform flow field. These effects are also included in the fin load calculation. Up to the limit angle of the fin data base, α_{limit} , the code uses the original (*M3F3CA*) equivalent angle of attack methodology, with the inclusion of angular rates and nonuniform flow field effects, to determine the loads on the missile's finned section. In most cases α_{limit} is 45°; however, for $M_\infty < 1.5$ it is 30°. Above α_{limit} , an approach is used based on the value of C_{NF} found at α_{limit} and the limit value at 90°. This approach is described in the fin force calculation section. The 90° limit is given by the drag coefficient of a flat plate normal to the flow (wing-alone value) determined by Hoerner.⁹ The newly available wing-alone data⁸ will provide additional data for determining better limit values at 90°. To allow for an increased fin normal force, over and above the flat plate value of Hoerner⁹ due to the presence of the body, factors are determined in a manner similar to that used by Aiello and Bateman.¹⁰

Body Force and Moment Calculations

To determine the loads acting on the body, the body is divided into segments. The load on each segment is determined including effects due to freestream, angular rates, and nonuniform flow fields. The following sections describe the body load calculation.

Angular Rates and Nonuniform Flow Field Effects.

In order to include the effects of angular rates and a nonuniform flow field, the body is divided into nose, fin, and afterbody sections. Each of these sections is divided into segments. Control points are fixed at the midpoints of each segment (on the centerline of the body). The local velocity induced by the angular rates ($u_{\text{rot}}/V_\infty, v_{\text{rot}}/V_\infty, w_{\text{rot}}/V_\infty$) is found for each segment control point by taking the cross product of the rotational rate vector (p, q, r) and the body control point position vector (x_b, y_b, z_b) as measured from the rotation center. Normalized perturbation velocities at the body

segment control points from a nonuniform flow field are added to the normalized angular velocities. The nonuniform flow field velocities are user-supplied. Forces and moments are calculated for each segment along the length of the body using the differential form of the equations developed by Jorgensen¹¹ shown below.

Potential Component of Body Load Calculation. The potential part of the normal force on the body is given in differential form by:

$$\frac{dC_N}{dx} = \frac{C_{N\alpha}}{2} \left[\frac{r_i^2}{r_b^2} \frac{d\alpha_i}{dx} \left(-\frac{1}{2} \sin 2\alpha_i \sin \frac{\alpha_i}{2} + 2 \cos \frac{\alpha_i}{2} \cos 2\alpha_i \right) + 2 \frac{r_i}{r_b^2} \frac{dr_i}{dx} \sin 2\alpha_i \cos \frac{\alpha_i}{2} \right] \quad (1)$$

where r_i is the body radius at the control point, r_b is the radius of the missile base, dr_i/dx is the body slope at the control point, and α_i is the local angle of attack for the segment determined from the sum of the freestream, angular, and nonuniform flow field velocities normal to the missile centerline. A similar equation can be written for the potential side force.

Crossflow Drag Component of Body Load Calculation.

If the freestream angle of attack is greater than 4°, the flow may separate. The axial location of the point of separation is determined from empirical relationships.¹ The crossflow drag contribution to normal force, in differential form, is calculated as follows for all control points aft of the point of separation.

$$\frac{dC_N}{dx} = 2\eta \frac{C_{dc}}{\pi} \frac{r_i}{r_b^2} \left[\left(\frac{w_i}{V_\infty} \right)^2 + \left(\frac{v_i}{V_\infty} \right)^2 \right]^{1/2} \frac{w_i}{V_\infty} \quad (2)$$

where C_{dc} is the crossflow drag coefficient and η is a correction factor for finite body length. Both are a function of crossflow Mach number, $M_c = M_\infty \sin \alpha_c$.

The factor η is a correction to two-dimensional cylinder data to account for the three-dimensional effects. It is a function of M_c and body fineness ratio, L/D . Following the method of Aiello and Bateman,¹⁰ the incompressible value of η is used up to $M_c = 0.8$ where it transitions to $\eta = 1.0$ at $M_c = 1.4$. As L/D increases, η increases. Table 3 shows η values used in *M3HAX* for 3 fineness ratios.

$M_c = M_\infty \sin \alpha_c$	η - factor for finite body length		
		L/D	
	1	12	40
0.0	.583	.700	.820
0.8	.583	.700	.820
0.9	.612	.721	.833
1.1	.792	.850	.910
1.3	.971	.979	.987
1.4	1.00	1.00	1.00
8.0	1.00	1.00	1.00

Table 3. η values vs. $M_c = M_\infty \sin \alpha_c$ and L/D.

Caution is required when comparing predicted values with sting-mounted wind tunnel data. The sting causes an effective increase in L/D.

The values of C_{dc} used are described by Jorgensen.¹¹ The data was modified around M_c 0.95 to 1.0 to lower the slope in C_{dc} to match other experimental data. *M3HAX* calculates C_{dc} based on M_c and crossflow Reynolds number, Re_c . Re_c is based on $V_\infty \sin \alpha_c$ and local body diameter. For $Re_c < 100,000$, the subcritical (higher) value of C_{dc} is selected for $M_c < 0.5$. The lower C_{dc} is used for $Re_c > 100,000$, supercritical flow. For $M_c > 0.5$, the two curves are identical. The values for C_{dc} used in *M3HAX* are shown in the table below:

M_c	C_{dc} - crossflow drag coefficient	
	$Re_c > 100,000$	$Re_c < 100,000$
0.0	0.29	1.20
0.2	0.47	1.20
0.4	0.96	1.23
0.6	1.37	1.37
0.8	1.62	1.62
1.0	1.72	1.72
1.2	1.67	1.67
1.6	1.47	1.47
2.0	1.40	1.40
2.4	1.37	1.37
3.2	1.30	1.30
8.0	1.30	1.30

Table 4. C_{dc} values vs. M_c and Re_c

Fin Force and Moment Calculation

This section summarizes the fin force and moment calculation and the equivalent angle of attack methodology. Reference 1 provides a complete description of this methodology. The fin-on-body data bases within *M3HAX* contain C_{NF} for an $a/s_m = 0.5$ and vortex effects present in the experiment. To utilize these data bases for the prediction aerodynamic characteristics of other configurations, the equivalent angle of attack methodology is employed. The α_{eq} methodology relates the fin-on-body C_{NF} to that of the

wing-alone C_{NW} , and accounts for geometric and vortex scaling effects. *M3HAX* includes new modifications to α_{eq} to include effects due to rotational (p,q,r) and nonuniform flow field velocities. The α_{eq} methodology is depicted in Figure 2. The α_{eq} method described below is used up to the limit angle of the fin data base, α_{limit} to determine the loads on each fin. In most cases α_{limit} is 45°; however, for $M_\infty < 1.5$ it is 30°.

Fin Load Calculation for $\alpha_{limit} < \alpha_c < 90^\circ$. The following procedure is used to calculate the fin loads above the data base α_{limit} . For $\alpha_c > \alpha_{limit}$, the value of the fin C_{NF} at 90° is determined as described previously. A value of C_{NF} at α_{limit} is determined using the α_{eq} method described below. In addition, the slope $dC_{NF}(\alpha_c = \alpha_{limit})/d\alpha_c$ is determined. The C_{NF} slope at 90° is assumed to be zero. To obtain the C_{NF} at the desired angle of attack, a cubic fit between α_{limit} and $\alpha_c = 90^\circ$ is calculated which matches the slopes at the endpoints. The fit is used to compute the C_{NF} at the desired α_c .

Fin Load Calculation for $\alpha_c < \alpha_{limit}$. Below α_{limit} the α_{eq} methodology depicted in Figure 2 is used to determine the fin loads. The numbers in Figure 2 indicate the steps within the α_{eq} formulation to determine the final fin loads for the actual geometry and flow conditions of interest. This procedure is outlined below. For supersonic Mach numbers where the crossflow Mach number, $M_c = M_\infty \sin \alpha_c$, exceeds 0.3, nonlinear body compressibility factors are determined to account for local Mach number, M_1 , and dynamic pressure, q_1 , effects. These corrections are described in Ref. 1.

Step (1): For M_∞ , α_c , ϕ_f , AR, and λ of the fin being considered, C_{NF0} is determined from the fin-on-body stability data base ($a/s_m = 0.5$) by interpolation. Using the wing-alone C_{NW} corresponding to the M_∞ , AR, and λ , the equivalent angle of attack α_0 is determined as shown in Figure 2. This is the α_{eq} corresponding to $a/s_m = 0.5$ and contains the vortex effects inherently present in the experiments.

Step (2): The vortex effects present in the experiment are removed. The semi-empirical forebody vortex model in *M3HAX* is used to estimate and remove the vortex effects present in the experimental data. The $\hat{\alpha}$ (hat symbol) in Figure 2 indicates α_{eq} without vortex effects.

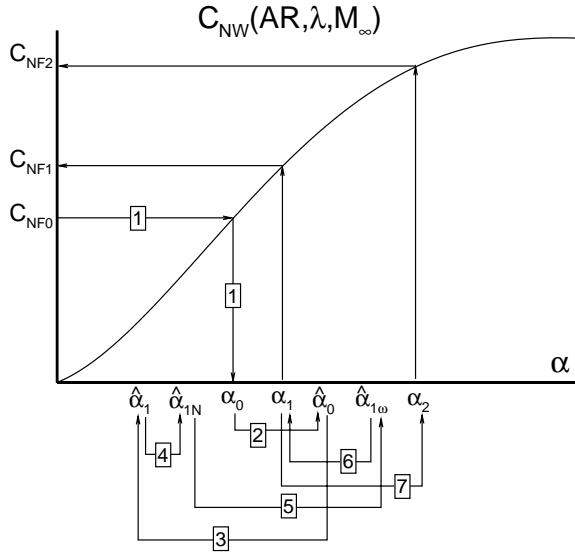


Figure 2.- Depiction of the Equivalent Angle of Attack Methodology.

Step(3): The α_{eq} is scaled from $a/s_m = 0.5$ to the actual a/s_m desired. This scaling assumes that the upwash is linear with respect to a/s_m .

Step (4): This step determines the change in α_{eq} due to a user specified nonuniform flow field. This information is read from an external file, and the user must specify the nonuniform perturbation velocities at each fin centroid. The velocity at the centroid is assumed to be representative of the nonuniform flow field over the fin.

Step (5): The effects of rotational rates (p,q,r) about the missile c.g. are added. The cross product of the rotational rate vector and the position vector to points on the fins is used to obtain the velocities due to rotation on the fin. The rotational velocity normal to the fin is used to obtain an increment in α_{eq} due to rotational rates.

Step (6): The effect of vortices present for the actual configuration and flow conditions of interest are added, α_1 . The vortex models used by *M3HAX* are described in the next section.

Step (7): The effects of fin deflections are added, α_2 . For transonic M_∞ , the Triservice control data base is employed. For supersonic M_∞ , interference effects and control effectiveness are handled by slender body theory.

Once the α_{eq} procedure has been carried out, the fin normal force is obtained from the wing-alone curve corresponding to the final values of α_{eq} . For a given

M_∞ , AR, λ , and C_{NF} , x_{CP}/c_R and y_{CP}/s are determined from the center of pressure data bases. With C_{NF} , x_{CP}/c_R and y_{CP}/s determined, the fin hinge- and bending-moment coefficients and the contribution of the fin loads to the overall force and moments can be calculated. See Ref. 1 for a more complete description of the α_{eq} method and the fin force and moment calculation.

Vortex Modeling in *M3HAX*

There are three vortex models contained in the *M3HAX*¹ and *M3F3CA* codes.² The forebody vortex model is used to obtain the vortex field influencing the first fin set. A fin vortex model is required to shed vorticity from upstream fins sets which influence the loads on aft fin sets, and an afterbody vortex shedding model is required to shed and track all vorticity along the body between fin sets. These models are described in detail in Refs. 1 and 2. For *M3HAX* the body vortex shedding and tracking model has been modified to include the effects of the nonuniform flow field and rotational rates. This amounts to including a doublet term which accounts for the local nonuniform flow and rotational velocity at each body segment. An example of a vortex field obtained with the *M3HAX* code is shown in the results section.

RESULTS

This section presents results obtained with the missile aerodynamics prediction method *M3HAX*. Comparisons of the results to experimental data are made for code verification and to indicate areas of improvement. Comparisons to experiment for single fin set and two fin set configurations are presented. In addition, the capability of *M3HAX* to predict lateral-directional aerodynamic characteristics for asymmetric flow conditions and fin deflections is also presented. Predictions of aerodynamic loads of a body-alone and a single fin set are presented up to 90° angle of attack. The prediction of roll and pitch damping derivatives is also demonstrated, as well as an example prediction of the nonlinear behavior of the pitch and roll damping at high α .

Single Fin Set Predictive Capability, $\alpha_c < 30^\circ$

M3HAX has been compared to the new fin-on-body data base of Ref. 8. This data base consists of 12 test fins shown in Figure 3. The AR (2 fins joined at root) range is 0.67 to 6. The body radius to fin semispan ratio, a/s_m , varied from 0.25 to 0.50. The hinge line was located at the 60% c_R location for all fins. The M_∞ range of the test program was 0.6 to 3.96 with an α_c

range from -2° to 30° . The model configuration was planar. Only zero roll angle was tested. The body consisted of a 3-caliber ogive nose with a total length of 12 diameters. The moment center for C_m was 7 diameters aft of the nose tip.

Figure 4 compares measured and predicted aerodynamic characteristics of the body/Fin 1 combination ($AR=2$, $\lambda=0.0$, $a/s_m=0.5$) for $M_\infty = 1.2$. The fin normal force, C_{NF} , and the bending moment, C_{BM} , are predicted very well including the effects of fin deflections (Fig. 4(a) and (c)). The fin hinge moment, C_{HM} , is in fair agreement (Fig. 4(b)). At transonic M_∞ , the fin hinge moment can be sensitive to the fin thickness distribution. The fins in the Triservice data base in *M3HAX* have double wedge sections. The fins of Ref. 8 are flat with beveled leading and trailing edges (modified double wedge). The overall configuration normal force, C_N , is predicted well as are the pitching moment and the axial force trends (Fig. 4(d), (e), and (f)).

Figure 5 compares measured and predicted aerodynamic characteristics of the body/Fin 12 combination ($AR=2$, $\lambda=0.5$, $a/s_m=0.25$) for $M_\infty = 1.2$. The fin and overall aerodynamic characteristics of this fin-body configuration are predicted very well at this M_∞ .

Comparisons of *M3HAX* to other configurations and flow conditions of Ref. 8 indicate that *M3HAX* does an excellent job of estimating overall and fin loads for conventional missile/fins configurations for preliminary analysis and design. Discrepancies in the predicted and measured hinge moments are seen in the transonic range. For some planforms, the effect of deflection is slightly underpredicted in the M_∞ range from 1.6 to 2.3.

Figure 6 gives a broader view of the predictive capabilities of *M3HAX*. The predicted and measured fin normal force is shown for all 6 trapezoidal fins (Fins 4,5,6,10,11,12, $\lambda=0.5$) for $M_\infty = 0.9, 1.2, 2.3$, and 3.95. The overall conclusion is that *M3HAX* predicts the fin normal force well over a wide range of flow conditions. However, some details between the measured and predicted results are of interest. For Fins 4, 5, and 6, the measured data show a dramatic C_{NF} stall at $\alpha = 8-10^\circ$ for $M_\infty = 0.9$. While *M3HAX* shows a nonlinear C_{NF} behavior at the same angles, the prediction does not capture the abrupt changes.

Two Fin Set Predictive Capability, $\alpha_c < 30^\circ$

Longitudinal Characteristics. Figure 7 compares measured¹² and predicted longitudinal results for a canard fin-controlled model at $M_\infty = 2.5$ with and

without 5° pitch control. The overall C_N , C_m , and C_A are predicted well.

Lateral-Directional Characteristics. Figure 8 compares measured¹² and predicted rolling moment characteristics for the same canard fin-controlled model at $\phi = 26.6^\circ$ for $M_\infty = 1.75$ and 2.5. This is an asymmetric flow condition with asymmetric fin deflection. Figure 8(a) shows predicted and measured results at $M_\infty = 1.75$ with canard fins 2 and 4 deflected $+5^\circ$ and -5° , respectively, for roll control. The tail-fin-off rolling moment prediction agrees well with the measured data. *M3HAX* does a reasonable job of predicting the complete configuration rolling moment.

Figure 8(b) shows predicted and measured results on the same configuration at $M_\infty = 2.5$ and $\phi = 26.6^\circ$ with roll control. The rolling moment prediction by *M3HAX* is reasonable. A comparison of Figures 8(a) and 8(b) indicates that both the experimental results and the *M3HAX* predictions show a significant Mach number effect on the rolling moment. The tail-fin-off rolling moment prediction agrees well with the measured results. The body shed vortices have a large effect on predicting the tail fin-induced rolling moment. Figure 8(c) depicts the predicted fin and body vortices at the tail fin leading edge for $M_\infty = 2.5$, $\alpha_c = 15^\circ$, and $\phi = 26.6^\circ$.

Predictive Capability Up To 90° Angle Of Attack

Body Alone Comparisons. In Figure 9, *M3HAX* results are compared to experiment¹⁰ for a body alone configuration with a tangent ogive nose and a fineness ratio 10. The potential body normal force slope, $C_{N\alpha}$ (see Eqn. 1), is set to 2.0, 2.5, 2.0, and 3.3 for Mach numbers 0.6, 1.15, 2.0, and 2.0, respectively. The $C_{N\alpha}$ affects the body potential force calculation most in the low angle of attack range where the viscous force term is small. The values for $C_{N\alpha}$ were determined from the experimental data at low angle of attack.

In Figure 9(a), the prediction is low up to an angle of attack of about 42° , where it becomes somewhat high up to 90° angle of attack. Figure 9(a) also presents data for $\eta = 1.0$ (see Eqn.2). The factor η is a correction which accounts for end effects and fineness ratio of the body. In Figure 9(b) for freestream Mach 1.15, the prediction is low up to 65° after which it slightly overpredicts the data. In Figure 9(c) for Mach 2.0, the $C_{N\alpha} = 3.3$ matches the data well. Figure 9(c) also presents a prediction for the input $C_{N\alpha} = 2.0$. For this case, the prediction is slightly low up to 40° and provides good agreement up to 90° . For preliminary analysis and design, *M3HAX* predicts body alone loads well.

Body-Tail Comparisons. Figures 10 and 11 show *M3HAX* predicted results compared with experimental data⁷ for total normal force, C_N , pitching moment, C_m , and fin normal force, C_{NF} , for a body-tail model at $M_\infty = 0.6$ and 2.5, respectively. Results are shown for angles of attack up to 90° with zero roll angle. The total normal force results at $M_\infty = 0.6$ (Fig. 10(a)) show fairly good agreement over the whole range of angle of attack. The fin normal force (Fig. 10(c)) shows a slight overprediction, mainly in the region from 50° to 90° . This effect shows in the pitching moment comparison (Fig. 10(b)); however, the maximum error in center of pressure is less than 0.5 of a body radii. The results at Mach 2.5 (Fig. 11) compare fairly well with experimental data for the overall normal force (Fig. 11(a)), pitching moment (Fig. 11(b)), and fin normal force (Fig. 11(c)). The fin normal force has a maximum error of 20% at 70° . The error in center of pressure location is 1.4 body radii at $\alpha = 20^\circ$, and the error is 0.9 body radii at $\alpha = 50^\circ$.

Roll Damping Derivative Prediction

Figure 12 compares the roll damping coefficient, C_{lp} , predicted by *M3HAX* with that predicted by the theoretical method of Adams and Dugan.¹³ The quantity $-C_{lp}/AR$ is plotted against the ratio of body diameter to overall span (d/b). As d/b approaches a value of 1.0, the overall span becomes equal to the body diameter (i.e., there are no fins) and the roll damping coefficient goes to zero. Results are given for cruciform and planar configurations. The *M3HAX* results show the same trends as Adams and Dugan's method for both cruciform and planar configurations. The magnitude of the roll damping coefficient is somewhat lower than Adams and Dugan's prediction. The fin aspect ratio for all cases was 2.0. The fin aspect ratio is based on two fins joined at the root. The body diameter was changed which in turn changed d/b (a/s_m) and aspect ratio. Note that this aspect ratio as plotted in Figure 12 is based on the fin area extended through the body covered by the root chord.

Pitch Damping Derivative Prediction

M3HAX predicts the full pitch damping derivative, $C_{mq} + C_{m\alpha}$, based on empirical methods.¹⁴⁻¹⁶ Values of wing lift-curve slope required by these methods are obtained from the wing-alone data base incorporated in *M3HAX*. Pitch damping results, C_{mq} , are also presented.

The measured and predicted pitch plane dynamic derivatives for the single fin set configuration are shown in Figure 13. The full pitch plane dynamic derivative, $C_{mq} + C_{m\alpha}$, predicted by *M3HAX* is shown with

experimental results taken from Ref. 17 for two center of gravity locations. The predictions overestimate the measured values; however, the trends are predicted reasonably well. Also shown is the pitch damping coefficient, C_{mq} , deduced from differencing the pitching moments calculated by *M3HAX* for the case of the body-tail model at zero angle of attack and a pitch rate, q . The values of C_{mq} alone, calculated from *M3HAX*, are not directly comparable, but repeat the trends well. These results indicate that the derivative $C_{m\alpha}$ should be negative in these cases.

The measured and predicted pitch plane dynamic derivatives for a two fin set configuration¹⁸ are shown in Figure 14. Both the magnitude and trend of the prediction are in reasonable agreement with experiment over the supersonic flow regime. The *M3HAX* prediction in the transonic flow regime is not predicted well since values are obtained by interpolating between subsonic and supersonic flow methods. However, it is considered suitable for preliminary analysis and design purposes.

Angular Rate Effects at High Angles of Attack

Because the angular rate effects (p, q, r) are included in the equivalent angle of attack methodology, *M3HAX* can be used to determine the nonlinear behavior of damping derivatives as a function of angle of attack. For engineering-level prediction codes, this is a unique capability of the *M3HAX* program. Figures 15 and 16 depict the roll damping, C_{lp} , and pitch damping, C_{mq} , coefficients as a function of angle of attack for Mach numbers 0.9 and 2.5. The configuration is the body-tail model depicted in Figure 10. The nonlinear behavior of the damping coefficients at transonic speeds is due in part to the nonlinear fin normal force behavior (see Fig. 10(c)). Figures 15 and 16 indicate that the damping at high angles of attack reduced 40%.

CONCLUSIONS

A fast and efficient aerodynamic prediction program, *M3HAX*, has been developed for missiles at speeds up to $M_\infty = 5.0$ and at angles of attack up to 90° . It is applicable to configurations having axisymmetric bodies with up to three finned sections. Roll angle is arbitrary. *M3HAX* also has the capability of predicting the effects of angular rates and nonuniform flow fields.

The extensive comparisons of measured and aerodynamic characteristics predicted by program *M3HAX* presented for verification purposes prompt the following observations. The code is capable of predicting the longitudinal and lateral-directional

aerodynamic characteristics of conventional missile configurations as well as the axial force and the pitch plane stability derivatives for an extensive range of flow conditions. Angles of attack up to 90° are permitted. Generally, predicted individual fin loads are in good agreement with experiment, and overall aerodynamic forces and moments are adequately predicted for preliminary design purposes. This is the prime objective of the new *M3HAX* code. Predicted results for high angles of attack ($\alpha_c > 30^\circ$) show reasonable agreement with experiments for all Mach numbers. The predicted effect of angular rates in pitch and roll were compared with experimental data and other methods.

M3HAX is fast running and has application in preliminary missile design and optimization. For a body-tail configuration, 432 flow conditions can be analyzed in 30 CPU seconds on a Hewlett-Packard 735 workstation. Cases involving afterbody vortex shedding and tracking consume more time, but still fit within the time constraints imposed by preliminary design and application in aerodynamic shape optimization programs.

A subroutine version of *M3HAX* has been developed which can be called from store separation codes. The nonuniform flow field from the parent aircraft is included in the loads calculations within *M3HAX*. The predicted forces and moments are then passed back to 6 degree-of-freedom trajectory simulation of the store release. This capability provides an improved level of aerodynamic prediction capability for store separation analyses.

RECOMMENDATIONS / IMPROVEMENTS

The first and most important recommendation is for additional testing and verification of the *M3HAX* code to better define the limits of its capability. Several areas for improvement include:

1. Improve the fin hinge moment prediction by including additional empirical information and/or correlations for the effects of different airfoil sections.
2. Extend the correlations for fin control effects through the incorporation of additional available control data.
3. Extend the method to include effects of changing missile afterbody radius, i.e., body flares and boattails.

REFERENCES

1. Lesieutre, D. J., Love, J. F., and Dillenius, M. F. E.: *M3HAX* Aerodynamic Analysis for Finned Vehicles with Axisymmetric Bodies. NEAR TR 493, February 1996.
2. Lesieutre, D. J., Dillenius, M. F. E., and Whittaker, C. H.: *M3F3CA* Aerodynamic Analysis for Finned Vehicles with Axisymmetric Bodies. NEAR TR 424, May 1991.
3. Lesieutre, D. J., Mendenhall, M. R., Nazario, S. M., and Hemsch, M. J.: Prediction of the Aerodynamic Characteristics of Cruciform Missiles Including Effects of Roll Angle and Control Deflection. NEAR TR 360, Revised August 1987.
4. Lesieutre, D. J., Mendenhall, M. R., and Dillenius, M. F. E.: Prediction of Induced Roll on Conventional Missiles with Cruciform Fin Sections. AIAA Paper No. 88-0529, January 1988.
5. Allen, J. M., Shaw, D. S., and Sawyer, W. C.: Analysis of Selected Data From The Triservice Missile Data Base. AIAA Paper No. 89-0478, January 1989.
6. Stallings, R. L., Jr., and Lamb, M.: Wing-alone Aerodynamic Characteristics for High Angles of Attack at Supersonic Speeds. NASA TP 1889, July 1981.
7. Baker, W. B., Jr.: Static Aerodynamic Characteristics of a Series of Generalized Slender Bodies With and Without Fins at Mach Numbers from 0.6 to 3.0 and Angles of Attack from 0 to 180°. AEDC-TR-75-124, Vol. II, May 1976.
8. Allen, J. M., Hemsch, M. J., Burns, K. A., and Deters, K. J.: Parametric Fin-Body and Fin-Along Database on a Series of 12 Missile Fins, Proposed NASA TM, May 1996 - to be published.
9. Hoerner, S. F.: Fluid Dynamic Drag. Published by Author, 1965.
10. Aiello, G. F. and Bateman, M. C.: Aerodynamic Stability Technology for Maneuverable Missiles. Vol. I, Configuration Aerodynamic Characteristics. AFFDL-TR-76-55, Vol. I, March 1979.
11. Jorgensen, L. H.: Prediction of Static Aerodynamic Characteristics for Slender Bodies Alone and with Lifting Surfaces to Very High Angles of Attack. NASA TR R-474, September 1977.
12. Blair, A. B., Jr., Allen, J. M., and Hernandez, G.: Effect of Tail Fin Span on Stability and Control Characteristics of a Canard Controlled Missile at Supersonic Mach Numbers. NASA TP 2157, June 1983.

13. Adams, G. J. and Dugan, D. W.: Theoretical Damping in Roll and Rolling Moment due to Differential Wing Incidence for Slender Cruciform Wings and Wing-Body Combinations. NACA Report 1088, 1952.
14. Ericsson, L. E.: Effect of Mach Number on Slender Vehicle Dynamics. AIAA Paper No. 80-0362, 1980.
15. Ericsson, L. E.: Modification of Aerodynamic Prediction of the Longitudinal Dynamics of Tactical Weapons. LMSC-D646354, 1979.
16. USAF Stability and Control Datcom Manual. April 1978.
17. Vukelich, S. R., Stoy, S. L., Burns, K. A., Castillo, J. A., and Moore, M. E.: Missile Datcom, Volume I, Final Report. AFWAL-TR-86-3091, December 1988.
18. Brown, A. E.: A Summary of Aerodynamic Data for Sidewinder 1C. NWC TN 4063-202, August 1967.

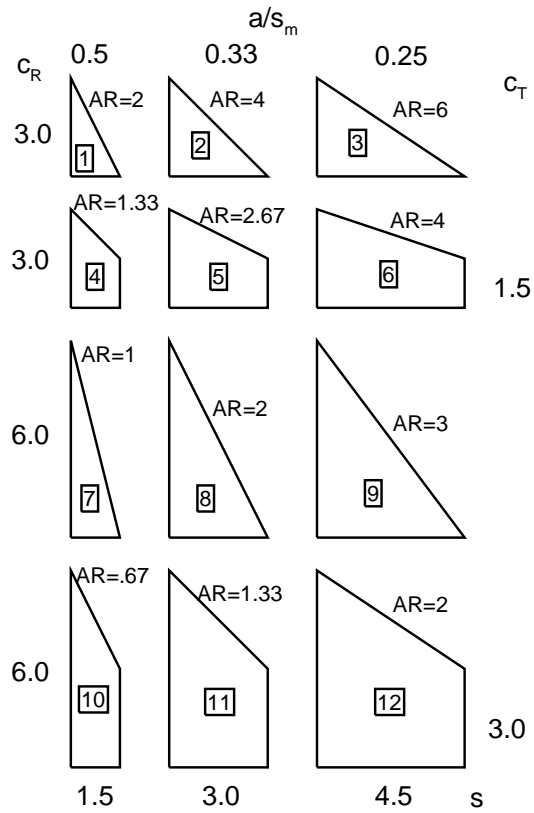
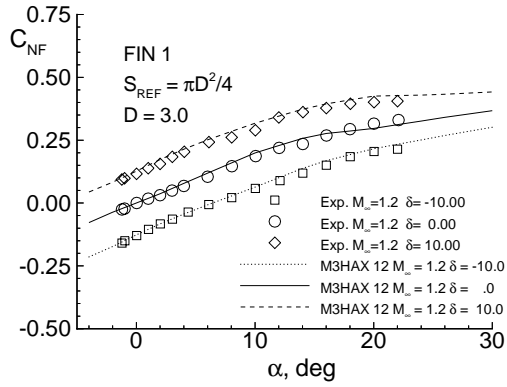
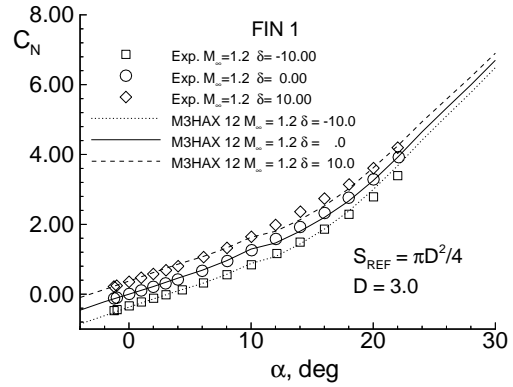


Figure 3.- Fins in Ref. 8 data base

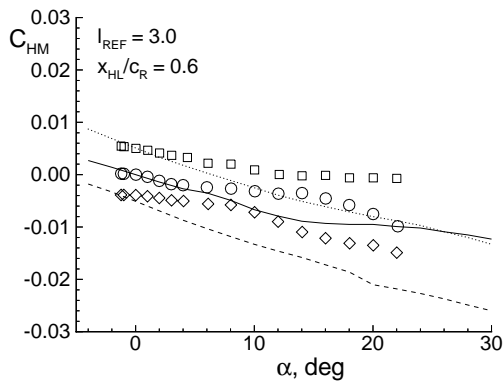
Figures continued on Page 10.



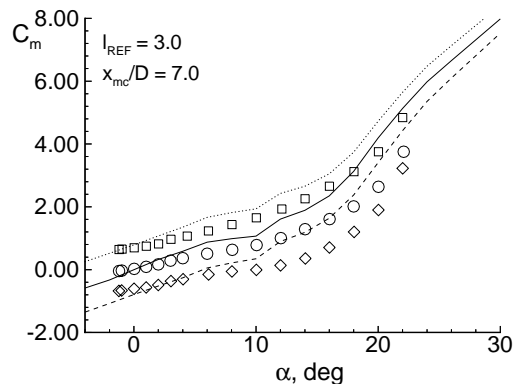
(a) Fin Normal Force



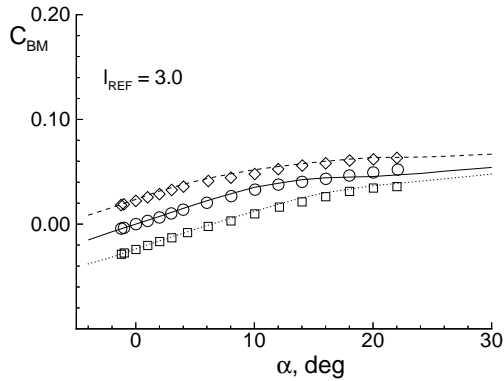
(d) Overall Normal Force



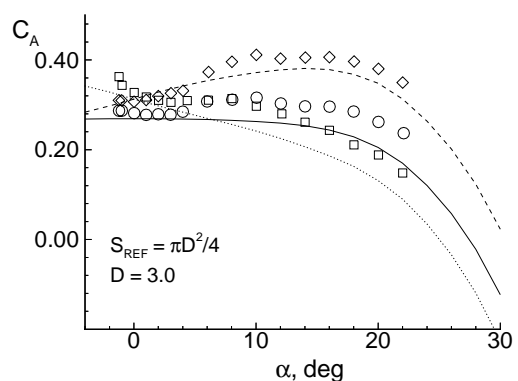
(b) Fin Hinge Moment



(e) Overall Pitching Moment



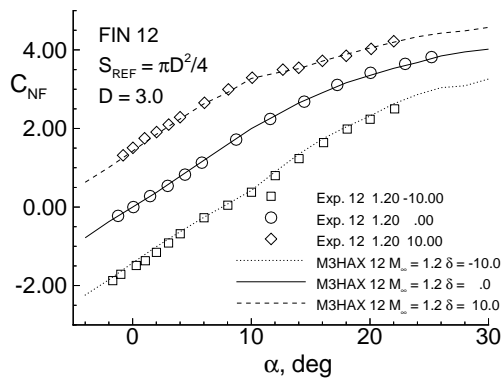
(c) Fin Bending Moment



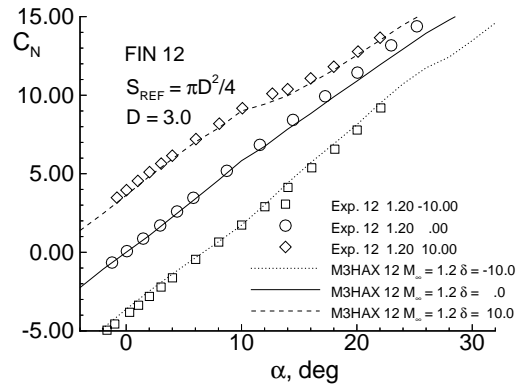
(f) Overall Axial Force



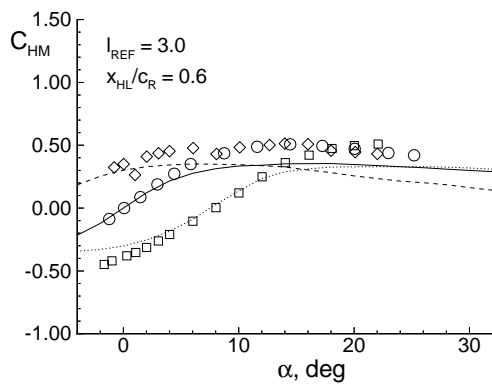
Figure 4.- Comparison of measured and predicted fin and overall aerodynamic characteristics of the fin-body configuration of Ref. 8, Fin 1, AR=2, $\lambda=0$, $a/s_m=1/2$, $M_\infty=1.2$.



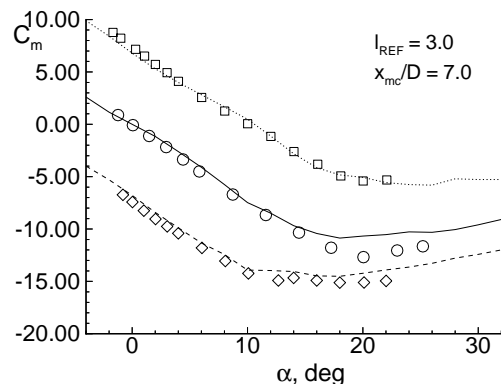
(a) Fin Normal Force



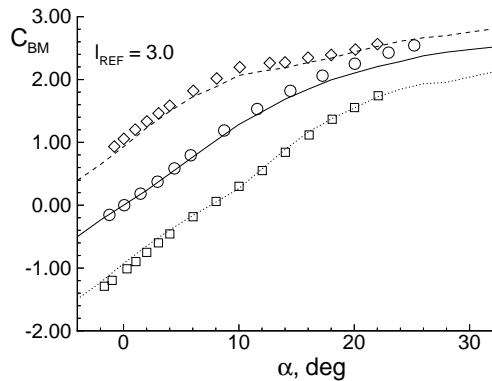
(d) Overall Normal Force



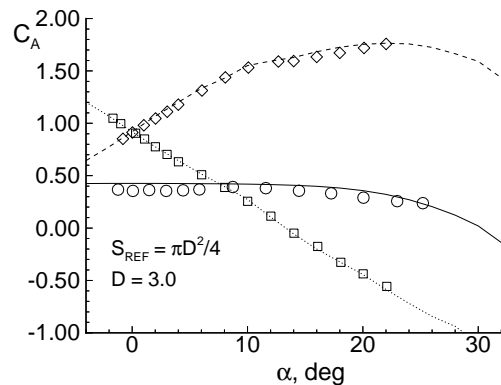
(b) Fin Hinge Moment



(e) Overall Pitching Moment



(c) Fin Bending Moment



(f) Overall Axial Force

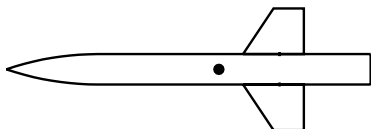
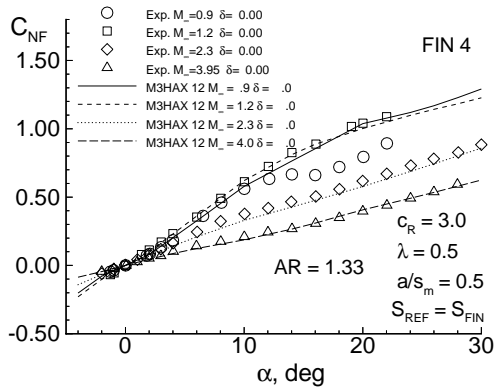
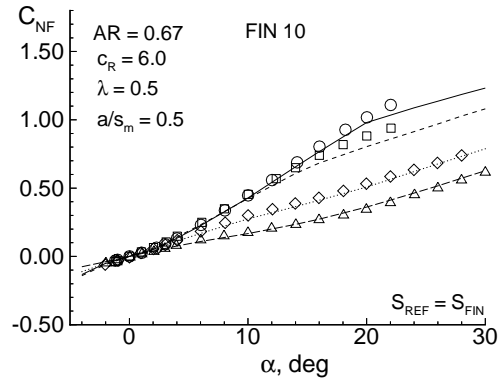


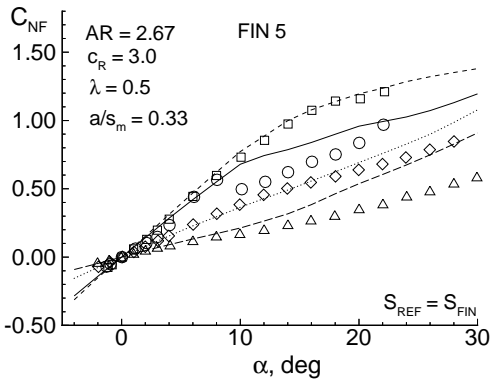
Figure 5.- Comparison of measured and predicted fin and overall aerodynamic characteristics of the fin-body configuration of Ref. 8, Fin 12 AR=2, $\lambda=1/2$, $a/s_m=1/4$, $M_\infty=1.2$.



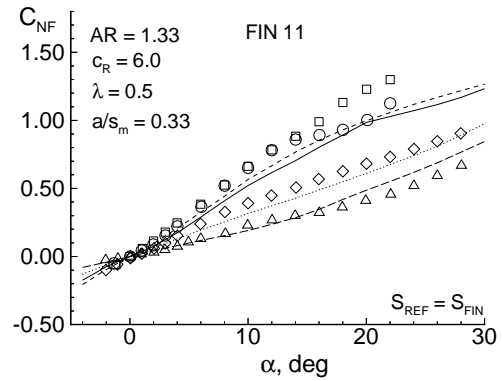
(a) Fin 4, $AR=1.33$, $\lambda=1/2$, $a/s_m=1/2$, $c_R=3.0$



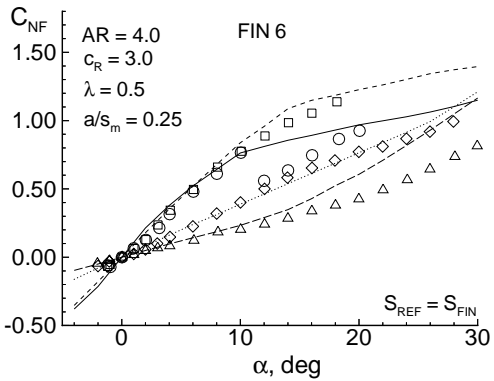
(d) Fin 10, $AR=0.67$, $\lambda=1/2$, $a/s_m=1/2$, $c_R=6.0$



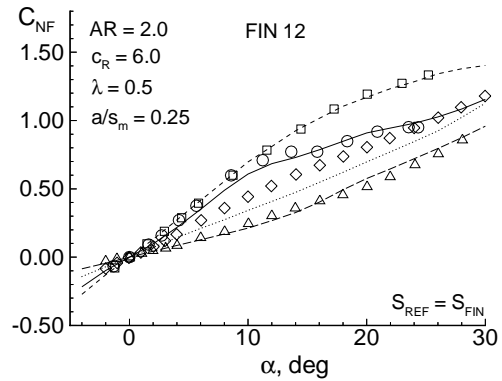
(b) Fin 5, $AR=2.67$, $\lambda=1/2$, $a/s_m=1/3$, $c_R=3.0$



(e) Fin 11, $AR=1.33$, $\lambda=1/2$, $a/s_m=1/3$, $c_R=6.0$

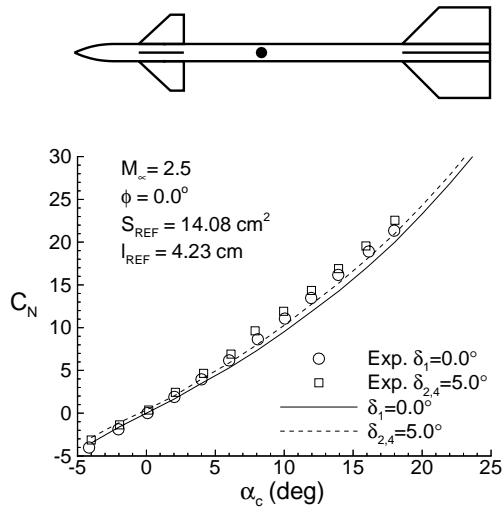


(c) Fin 6, $AR=4.0$, $\lambda=1/2$, $a/s_m=1/4$, $c_R=3.0$

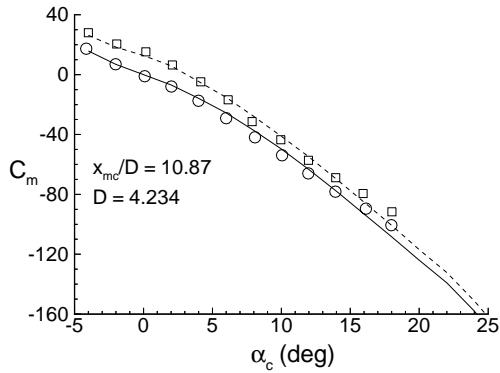


(f) Fin 12, $AR=2.0$, $\lambda=1/2$, $a/s_m=1/4$, $c_R=6.0$

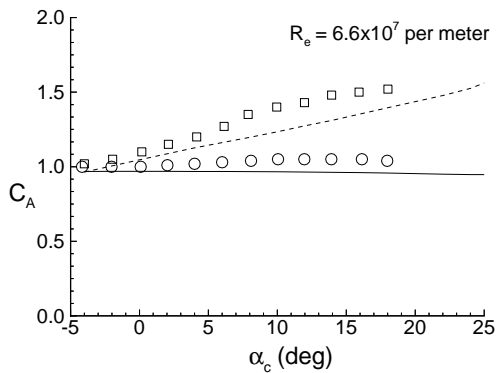
Figure 6.- Comparison of measured and predicted fin normal force characteristics of trapezoidal fins of Ref. 8 for $\delta = 0^\circ$.



(a) Overall Normal Force

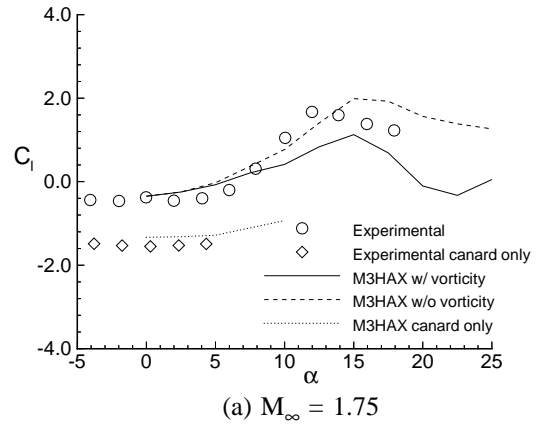


(b) Overall Pitching Moment

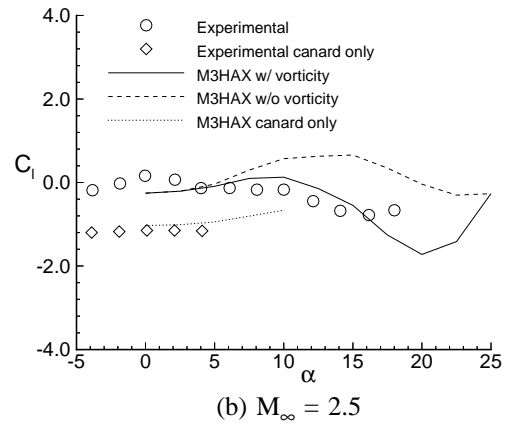


(c) Overall Axial Force

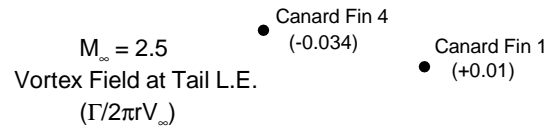
Figure 7.- Comparison of measured and predicted overall aerodynamic characteristics for the canard-body-tail model of Ref. 12, $M_\infty=2.5$, $\phi=0^\circ$, $\delta_{2,4}=0$ and 5° .



(a) $M_\infty = 1.75$

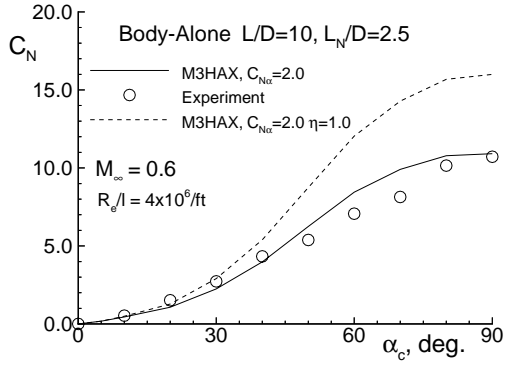
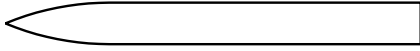


(b) $M_\infty = 2.5$

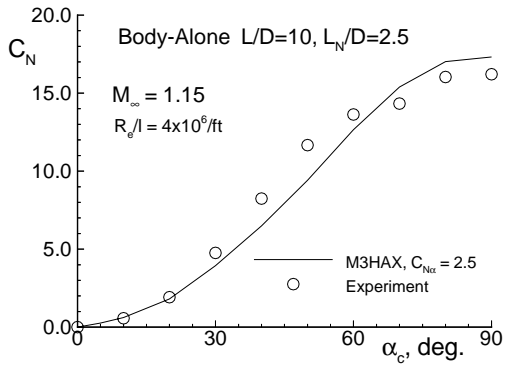


(c) Vortex Field at Tail Leading Edge
 $M_\infty=2.5$, $\alpha_c=15^\circ$, $\phi=26.6^\circ$, $\delta_{2,4}=\pm 5^\circ$

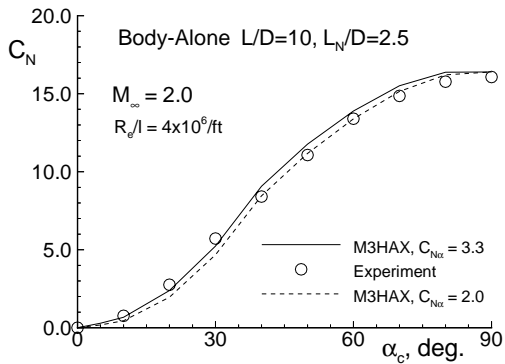
Figure 8.- Comparison of measured and predicted rolling moment characteristics for the canard-body-tail model of Ref. 12, $M_\infty = 1.75$ and 2.5 , $\phi=26.6^\circ$, and $\delta_{2,4}=\pm 5^\circ$ roll control.



(a) $M_\infty = 0.6$

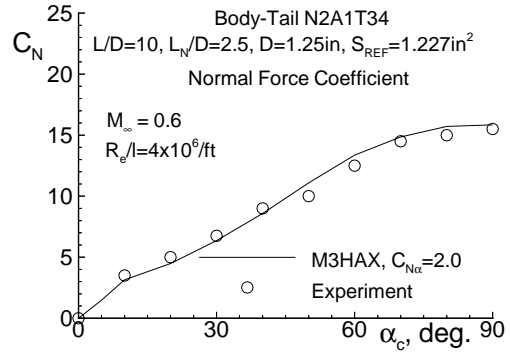
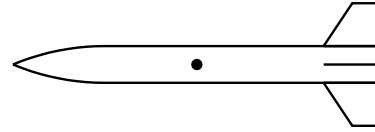


(b) $M_\infty = 1.15$

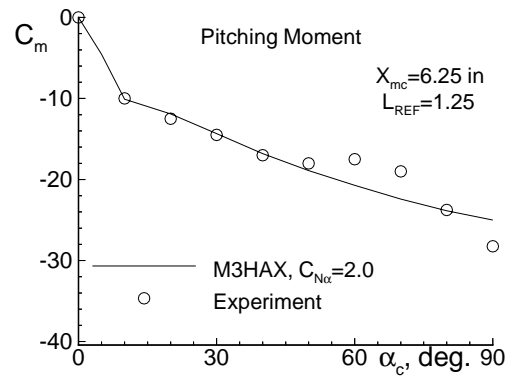


(c) $M_\infty = 2.0$

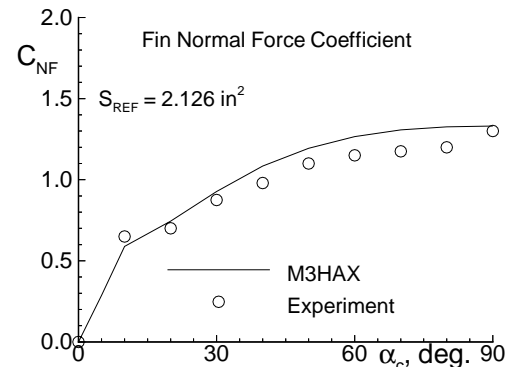
Figure 9.- Comparison of measured (Ref. 10) and predicted C_N for a body-alone.



(a) Overall Normal Force

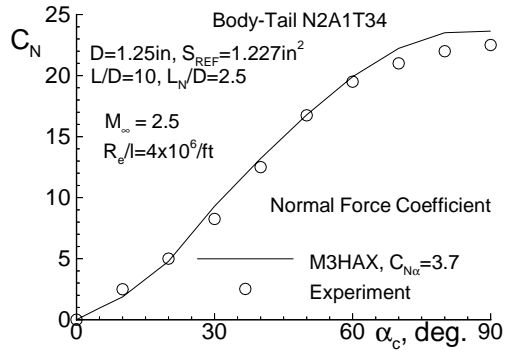
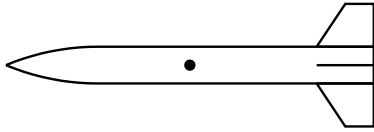


(b) Overall Pitching Moment

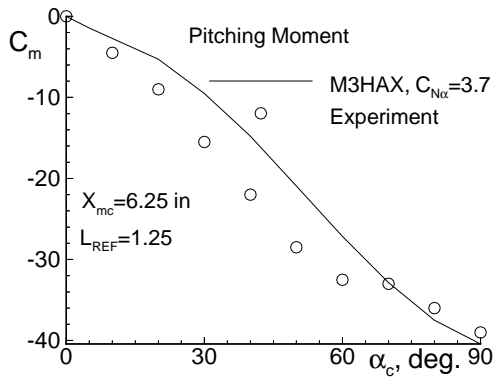


(c) Fin Normal Force

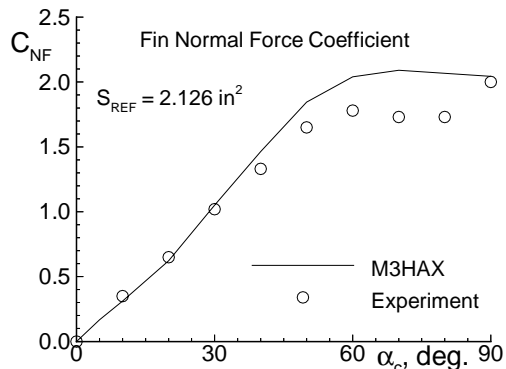
Figure 10.- Comparison of measured (Ref. 7) and predicted aerodynamic characteristics for a body-tail configuration, $M_\infty=0.6, \phi=0^\circ$.



(a) Overall Normal Force



(b) Overall Pitching Moment



(c) Fin Normal Force

Figure 11.- Comparison of measured (Ref. 7) and predicted aerodynamic characteristics for a body-tail configuration, $M_\infty=2.5$, $\phi=0^\circ$.

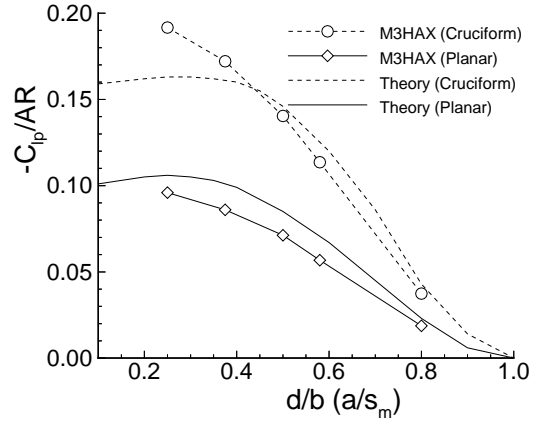


Figure 12.- Comparison of predicted C_{lp} with the theoretical values of Ref. 13.

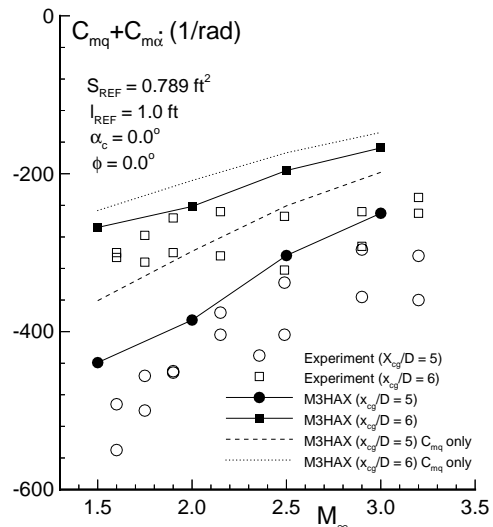
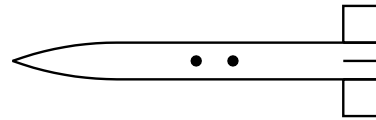


Figure 13.-Comparison of calculated C_{mq} with predicted and measured $C_{mq}+C_{m\alpha}$, Ref. 17.

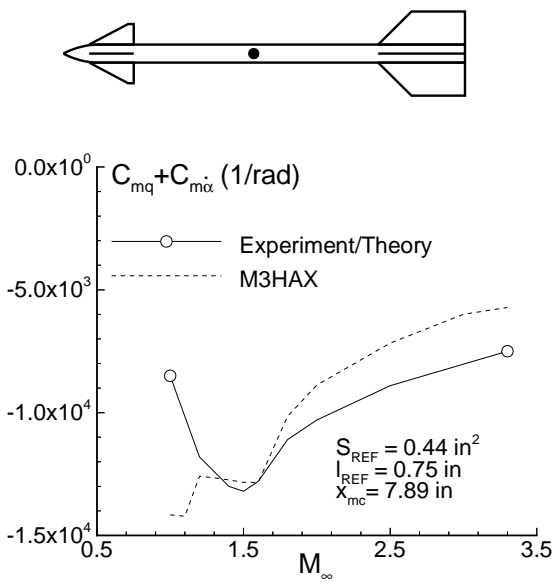


Figure 14.-Comparison of measured (Ref. 18) and predicted $C_{mq} + C_{m\dot{\alpha}}$ for a two fin set configuration, $\alpha_c = 0^\circ$, $\phi = 0^\circ$, $\delta_i = 0^\circ$.

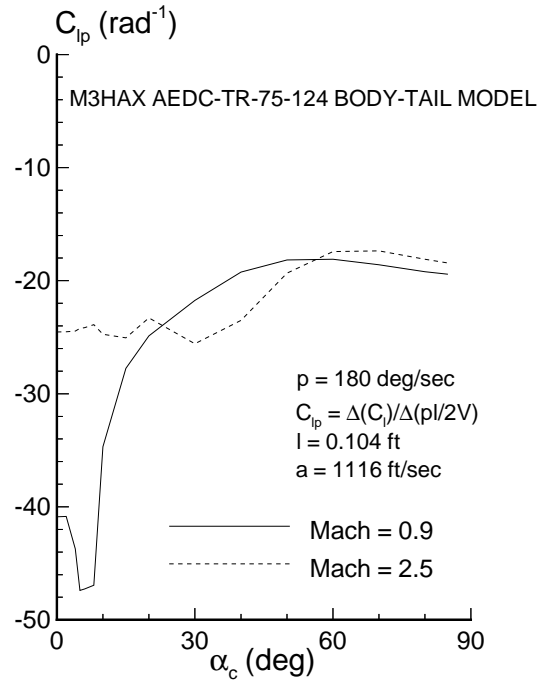


Figure 15.- *M3HAX* predicted roll damping as a function of α_c for the body tail of Ref. 7 (see Fig. 10).

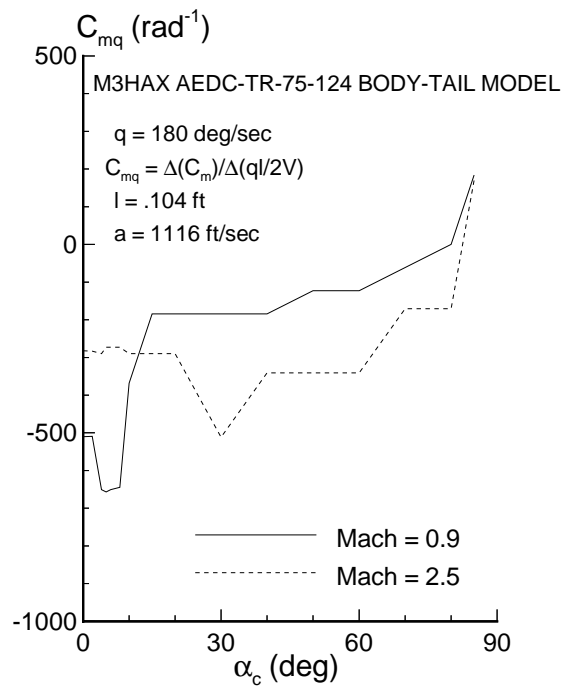


Figure 16.- *M3HAX* predicted pitch damping as a function of α_c for the body tail of Ref. 7 (see Fig. 10).